Precision synchronization for free-space quantum networking

Neal W. Spellmeyer*, Don M. Boroson, P. Benjamin Dixon, Matthew E. Grein, Nicholas D. Hardy, Catherine Lee, Ryan P. Murphy, Hemonth G. Rao, Marvin Scheinbart, Katia Shtyrkova, Mark L. Stevens, and Scott A. Hamilton
MIT Lincoln Laboratory, 244 Wood St., Lexington, MA USA 02421

ABSTRACT

Precision synchronization is vital for robust long-distance quantum networking over fiber and free-space channels for which high-fidelity entanglement swapping between separate sources via an optical Bell state measurement requires temporal overlap of photonic qubits arriving from either source. This challenge is particularly distinct in satellite-based entanglement distribution in which relative motion, channel effects, and propagation delay must be addressed. This work presents a precision synchronization method for free space entanglement distribution, and reports on risk reduction testing in a quantum networking testbed at MIT Lincoln Laboratory. Primary consideration is for a dual-uplink architecture in which photons from entanglement sources at two ground locations interact in an optical Bell-state measurement implemented on a satellite in a low-earth orbit. The control approach uses independent entanglement sources at each ground location supplemented with a synchronization signal for feedback control from a timing discriminant measured at the spacecraft. The approach is being implemented in a laboratory testbed using 1-GHz repetition rate 1550-nm band entanglement sources generating ~10-MHz source entanglement rates with few-ps photon pulse lengths. The paper describes both fundamental architectural considerations and practical implementation details.

Keywords: Precision Synchronization, Hong-Ou-Mandel, Phase-Locked Loop, Quantum Networking, Quantum Entanglement, Free-Space Communications

1. INTRODUCTION

A central challenge to high-rate entanglement distribution is establishing and maintaining precision synchronization of interacting photons originating from entanglement sources in different locations. In order to achieve high entanglement rates with good purity, source photons are often spectrally broad and correspondingly short in time [1], with ~1-ps photon durations leading to a need to synchronize to ~0.1 ps. This can be particularly challenging for long-distance satellite-based entanglement distribution for which photons need to be synchronized over 100-1000-km distances between platforms with ~7-km/s relative motion. This paper describes and implements a technique for realizing precision synchronization between sources that would be located at two different ground sites and interact at a satellite. Synchronization is achieved by feeding timing information measured at the satellite to the ground locations to close timing control loop.

The paper is structured as follows. Section 2 gives an overview of various space-ground link architectures applicable to quantum networking based on entanglement distribution, and outlines and quantifies the need for precision time/frequency synchronization due to satellite movement at various orbits of interest. Section 2 also provides an example of a particular implementation of a 'dual-uplink' architecture and an associated synchronization methodology. Section 3 describes a laboratory testbed that emulates the dual uplink architecture as well as the associated time and frequency effects on the signals due to satellite motion. The implementation of synchronization control is discussed in detail. Section 4 shows experimental results achieving <1-ps synchronization as the photon arrival time and frequency changes over a modest Doppler range and rate. Prospects for operation over larger Doppler ranges and rates are discussed

2. LINK ARCHITECTURE AND SYNCHRONIZATION CONTROL

Free-space satellite links present a compelling means for long-distance entanglement distribution because their distance-squared scaling can outperform the exponential loss presented by optical fibers [2]. Figure 1 shows three different link architectures. The dual downlink uses a single entangled photon source in space transmitting to users at two ground sites. Alternatively, the dual-uplink architecture [3] uses an entangled photon source at each ground terminal. One entangled photon from each source is sent over a free-space optical link to interact via an optical Bell state measurement (OBSM) at

* neal@ll.mit.edu

the spacecraft to create shared entanglement between the two ground terminals. The third architecture is the uplink/downlink in which entangled photon sources are located at each ground station. A photon from one source is relayed by the satellite to the other ground station, where it can interact with users in an OBSM. While each architecture has advantages and disadvantages in a system, the interesting and complex design trades between these three architectures are not the focus of this paper. Rather, this paper considers synchronization techniques having relevance to all three scenarios.

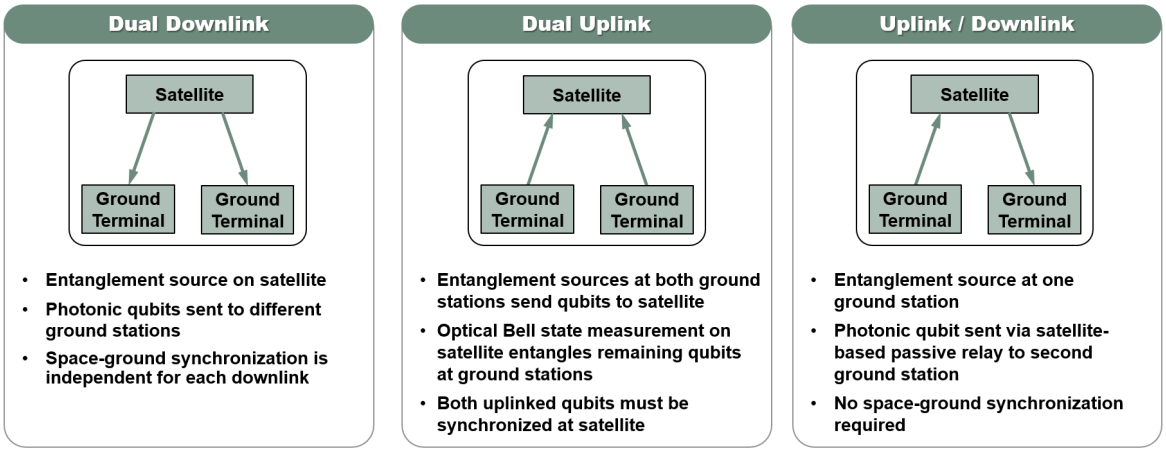

Figure 1 Three free-space entanglement distribution architectures that require precision synchronization. The dual downlink uses a single entangled photon source on the satellite, and sends photons to two ground receivers. The dual uplink uses entangled photon sources at the two ground sites. Photons interact at an OBSM at the satellite. The uplink/downlink architecture sends photons from one ground terminal to the other via the satellite, which acts as a pass through.

For these architectures, satellite motion creates a changing time of flight and a change in the apparent pulse repetition rate and photon wavelength when photons interact in the OBSM. These effects have different consequences depending on the durations of the photons used. Figure 2 shows Doppler profiles for representative LEO and MEO circular trajectories considered for the analysis in this work. For wideband (~1 ps) signals, the ~30-part-per-million Doppler shifts are negligible compared to the ~400-GHz optical bandwidth. However, the changing photon arrival times due to the changing optical path length are significant compared to the ~1-ps photon duration, indicating that temporal synchronization requires some form of a precision control approach, whereas dedicated wavelength control is unnecessary. The opposite becomes true for a 'narrowband' case such as that needed for interaction with emerging quantum memories that have relaxed timing constraints (e.g., ~10-100 ns) but narrow spectral bandwidths (~10-100 MHz) [7].

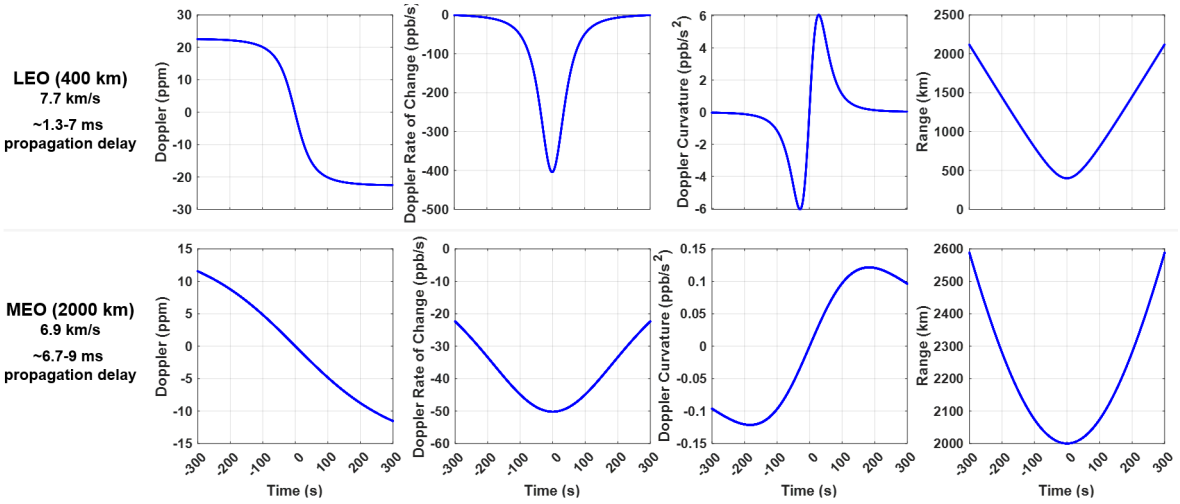

Figure 2 Doppler, Doppler rate of change, and Doppler curvature calculated for circular low-earth orbit (LEO) and medium-earth-orbit (MEO) trajectories, with ranges shown in the right-most panel. The Doppler range sets the control loop frequency throw, while the Doppler rate of change influences the allowable loop bandwidth. Units are in parts per million (ppm) and parts per billion (ppb).

Many authors have considered synchronization and related problems of ranging and time transfer for a variety of applications including quantum networking. Reference [4] considers clock synchronization using second order quantum coherence of entangled photons and optical delay lines to maintain synchronization. Comb-based optical time-frequency transfer [5, 6] has demonstrated exquisite capabilities over long-distance atmospheric links and to moving platforms while in some cases achieving near-quantum-limited sensitivity. The techniques described in this paper adapt elements of these concepts using sources and detectors in a novel way that can have dual use for the quantum networking functionality while reducing spacecraft resources and maintaining scalability to cases of large link loss and significant spacecraft motion.

Figure 3 shows the proposed control architecture for wideband synchronization in the dual-uplink architecture. The technique uses frequency-tunable sources at the ground sites to generate strong timing signals that are measured at the satellite to give good relative timing information about the signals from the two sources. This information is fed to the ground sites, where the laser pulse repetition rate is controlled to establish and maintain alignment of the signals at the satellite. This concept is driven by several considerations that will be discussed subsequently in the paper:

- Source repetition rate tuning is needed to address the large changes in path length due to orbital motion.
- Ground clock and laser sources that are less size, weight, and power (SWaP) constrained can carry the burden of good stability (low phase noise) with wide tunability. Much of the space-to-ground control loop processing can be implemented using ground resources.
- Use of a timing measurement that is a direct measure of the relative time of arrival of the photons from the two sources at the spacecraft detector. While many techniques are viable for this, the work implemented here uses a Hong-Ou-Mandel (HOM) interferometer that is part of the OBSM used for the entanglement distribution.
- Provision for an additional, strong synchronization signal. For a source with ~10-MHz entangled photon generation rate and ~20-dB link loss, the ~10^5 photons/s arriving at the spacecraft from each terminal are unlikely to provide sufficient signal for a control loop with sufficient bandwidth.
- Provision for local delay lines that could make fine timing corrections with fast bandwidth using timing information collected at the spacecraft.
- A low-latency communications channel (RF or optical) for sending timing information to one or both ground sites to be used for a control loop adjusting the source repetition rate to compensate for the large orbital motion.
- Provision for a fixed or variable timing offset between the synchronization signal and the quantum signal, permitting the control loop to lock using the strong slope on the side of the HOM dip while placing the quantum signal at the optimal center of the dip. An alternative but more complicated technique is to use dither-based control.

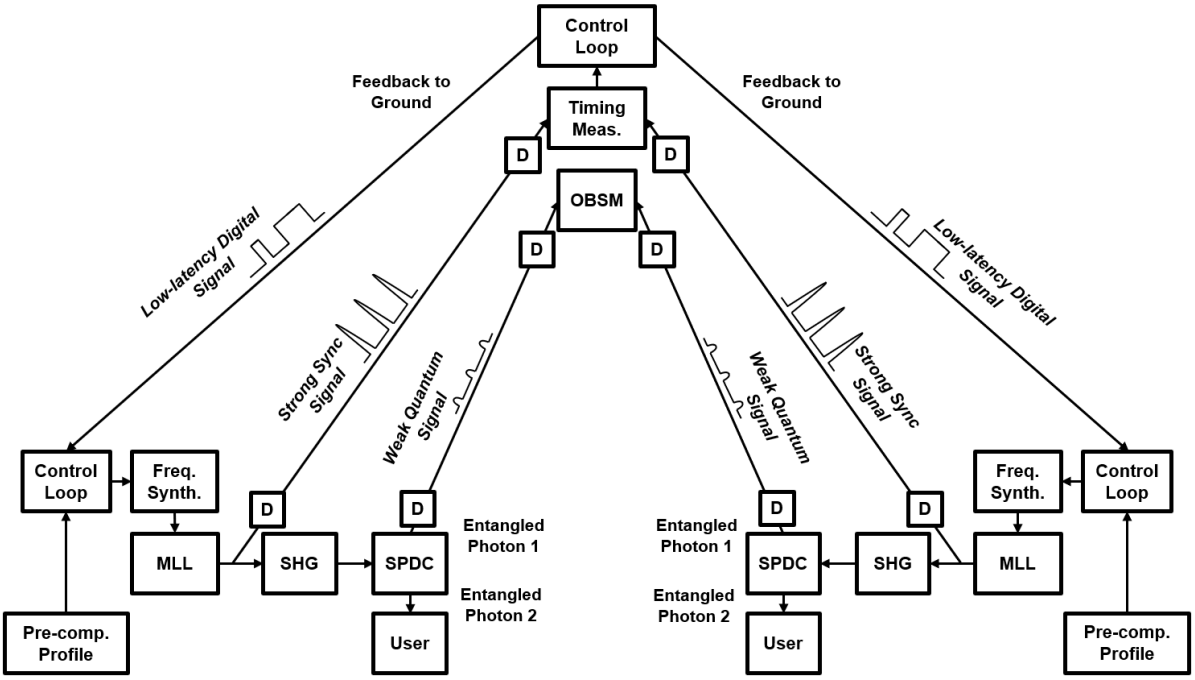

Figure 3 Synchronization control architecture. Spontaneous Parametric Down Conversion (SPDC) sources at two separate ground locations are pumped by photons from a second harmonic generation (SHG) stage fed from a mode-locked laser (MLL) whose repetition rate is controlled by a tunable synthesizer. A low-flux quantum signal from the entanglement source is combined with a stronger synchronization signal and transmitted from each ground terminal to separate apertures on a space terminal. The signals interact in an OBSM and a timing measurement. Synchronization information is fed via a low-latency digital channel to the ground terminals, where a control loop changes the MLL repetition rate by tuning a frequency synthesizer. There is provision for local tunable delay lines (D) that can support fast tuning mechanisms driven from local control loops as necessary to correct for fast but low-throw effects, and for fine alignment of the quantum signals relative to the synchronization signal. Doppler pre-compensation profiles can be fed to each terminal to reduce the overall control burden.

The atmosphere has several effects that must be considered. As the satellite moves across the sky, there is a change in the total atmospheric path length. This change in distance is small compared to the overall distance changes due to orbital motion, and can be corrected for via repetition rate control to adjust overall optical path length. Atmospheric jitter occurs on a range of time scales [8, 9]. While the round-trip control loop has limited control bandwidth, analysis shows that jitter effects on faster time scales (e.g. >10 Hz) are negligible compared with the ~1-ps optical pulse lengths. If such effects were significant, they could be corrected via local feedback control of the path length at the satellite, assuming sufficient flux exists to support a large control bandwidth. Other sources of jitter (e.g. mode-locked laser phase noise) can also be negligible depending on the source laser and reference clock stability. If necessary, these fast effects could also be corrected using fast, local adjustable path length delay, as described for the case of fast atmospheric jitter.

Atmospheric propagation introduces intensity variations on a ~1-kHz time scale, leading to a variation in the detected HOM coincidence rate used for the timing measurement. Because the received flux can be measured from the much larger 'singles' detection rate, the HOM timing discriminant can be normalized for the received flux. A detailed analysis of many different contributing effects is needed to fully evaluate performance in this situation.

In an implementation, there is a choice of how to control the frequency and phase of the two ground sources. Because the control loop needs to achieve overlap of the pulses at the satellite, the frequency difference of the two sources will correspond to the line-of-sight speeds of the two sources relative to the spacecraft. For example, one source could be set to a fixed frequency while the other tunes as needed. Alternatively, either or both sources could be pre-compensated to remove the line-of-sight Doppler, with residual errors corrected by the feedback control loop.

Although the particular implementation in this paper is focused on the dual uplink, the synchronization control techniques described and demonstrated here are applicable to other link architectures as well. For the uplink-downlink case, the space terminal serves as a signal pass-through, with all of the synchronization hardware located at the ground terminals. This

relaxes considerations about SWaP and space-qualification of the space terminal hardware needed for the dual-uplink, and net Doppler changes between the ground terminals will be smaller. For the dual-downlink, users at each downlink site can independently align their sources with the photons received on the downlink via frequency control of their sources. In this case, because the laser being tuned is co-located with the timing measurement, the control is not limited by a large round-trip time, and therefore can potentially be implemented with a faster loop bandwidth if there is sufficient incoming flux in the synchronization signal. With a faster loop bandwidth, it may be possible to use a simpler type-2 control loop (see discussion below), and there can be a greater tolerance for sources with poor phase noise at frequencies up to the loop bandwidth. Alternatively, a pump forwarding technique [10, 11] can be used to generate aligned user entangled photons.

3. LABORATORY SYNCHRONIZATION TESTBED

The dual uplink architecture and the proposed synchronization technique was implemented in a laboratory testbed as shown in Figure 4. The testbed has dual independent high-rate entanglement sources representing sources at two ground sites A and B. These sources are similar to those described elsewhere [1], and operate at a ~1-GHz slot rate, with a ~1-% slot occupation rate, yielding ~10-MHz source entanglement rate near 1550 nm. A strong classical pump signal is available at either 1550 nm or 775 nm. For this work focusing on synchronization, the 775-nm synchronization signal is used with the assumption that the space side of the system would operate near 775 nm to leverage, for example, efficient microchannel plate photomultiplier tube (MCP-PMT) detectors that would not require cryo-cooling needed for a superconducting nanowire single photon detector (SNSPD). Future work would be necessary to extend the entanglement source to generate pairs at these wavelengths. The testbed uses SNSPD detectors that can receive photons at either wavelength. The source MLL pulse repetition rate is fixed to a local reference clock generated by a stable but tunable frequency synthesizer via an analog phase locked loop with ~1-kHz control bandwidth.

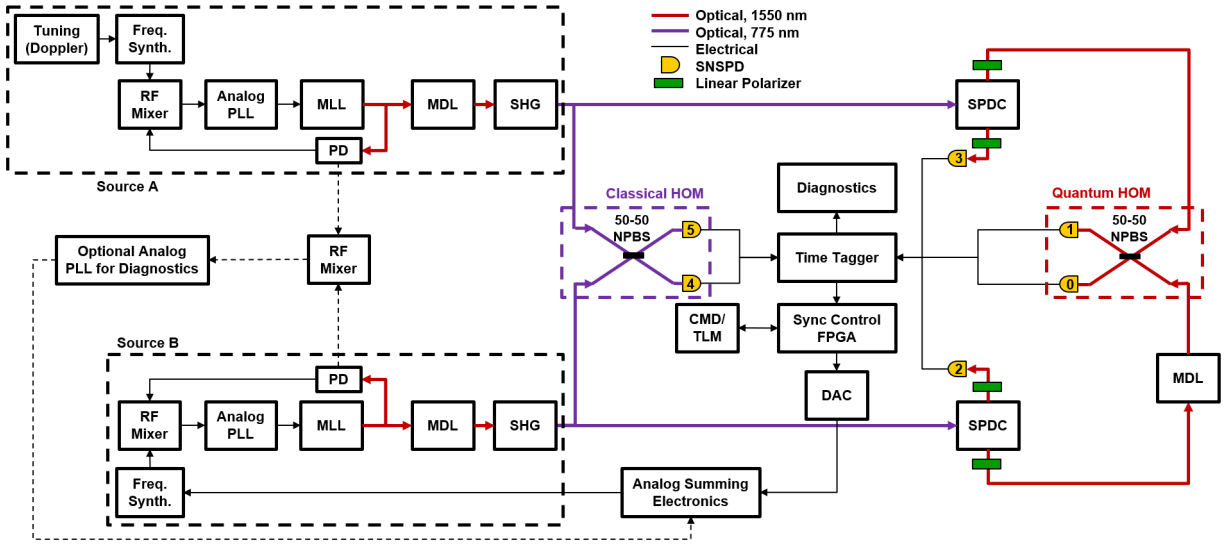

Figure 4 Synchronization testbed block diagram showing key functional elements. Source A and Source B and the SPDC sources represent functions at the two ground terminals. SHG converts the 1550-nm MLL output to 775-nm pulses. Some functions such as filtering and fiber amplification are not shown. The HOM functions plus time tagger represent space-side functions. Real-time time-tagger processing and feedback control loop processing occur in an FPGA. A feedback control voltage is generated in a 16-bit digital-to-analog converter (DAC) that feeds the frequency modulation control port of the Source B synthesizer. The testbed does not implement the digital communication needed to transfer the coincidence information to the ground terminal control. Fiber optic motorized delay lines (MDL) provide fine timing delay for some measurements, such as the HOM scans used in Figure 5 and Figure 8. PD represents a high-speed photodetector function internal to the MLL that detects the ~1 GHz MLL pulse repetition rate. Analog phase locked loops (PLL) control a tuning port in the MLLs to set their frequency to follow that of the frequency synthesizers with ~1 kHz bandwidth. An optional analog PLL is available to lock Source B to Source A using a strong local signal for diagnostic purposes (Figure 5) and is not used when the FPGA synchronization control loop operates. NPBS is a nonpolarizing fiber optic 50/50 beam splitter. A computer provides a command and telemetry (CMD/TLM) interface to the synchronization control FPGA.

The 775-nm pump light from each source is split off and directed into a 50/50 beam splitter followed by detection. This represents the space-side HOM interaction. Because this is a 'classical' HOM interaction, link loss can be overcome by transmitting a larger power at the source to achieve sufficient flux at the receiver. This strong synchronization signal could be combined with the weak quantum signal (with only ~1% slot occupation at the transmitter). The synchronization signal could be in band (i.e., at the same wavelength, obeying a frame structure) or out of band (i.e., at a different wavelength). The in-band method would be more robust against channel effects such as dispersion, although a near out-of-band signal should be viable. The design of a specific frame structure and its use for synchronization as well as the numbering and accounting of the entangled photon states that will be needed for the end-to-end quantum functions is beyond the scope of the work described here.

Photons from the two beam-splitter ports are detected (Quantum Opus SNSPDs) and time-tagged (PicoQuant MultiHarp 160). Time-tags pass into a Digilent Genesys 2 field-programable gate array (FPGA) where they are processed to generate a measure of total signal flux from both ports and the coincidence counts in a configurable timing window. As the arrival time of photons from one source changes relative to the other, the coincidence counts trace out a HOM dip which can be used to generate a timing feedback discriminant. Although the timing discriminant can in general be used for both low-throw fine-path-length control (e.g., via an optical delay line) at the space and/or ground terminals as well as frequency control at the ground sources, the method implemented here includes only frequency feedback control without actively controlling fine delay lines.

The space-to-ground propagation delay limits the control bandwidth. For a range of 400 km the round-trip time is 2.6 ms. This work uses a 10-ms control update rate as an approximate representation of the round-trip latency. There is also provision in the FPGA for a delay buffer, which is practical to implement given the relatively small volume of digital coincidence count information. Future testing can explore performance vs. round-trip delay, which is important given the potential for instabilities in the type of control loops investigated here. The Doppler-induced frequency shift resulting from spacecraft motion can be emulated by frequency tuning of the sources. Other effects, such as fast power fluctuations resulting from atmospheric effects, can also be represented here, although that has not yet been implemented in the testing.

4. EXPERIMENTAL RESULTS

While the goal of this work is to achieve synchronization with realistic LEO Doppler profiles, initial testing of the timing discriminant occurred with both sources locked to a common clock via an analog phase-locked loop. The timing discriminant was then characterized by scanning the delay of one source relative to the other with a tunable optical delay line while recording the classical HOM coincidence dip with an expected 50% maximum visibility [12-15]. See Figure 5.

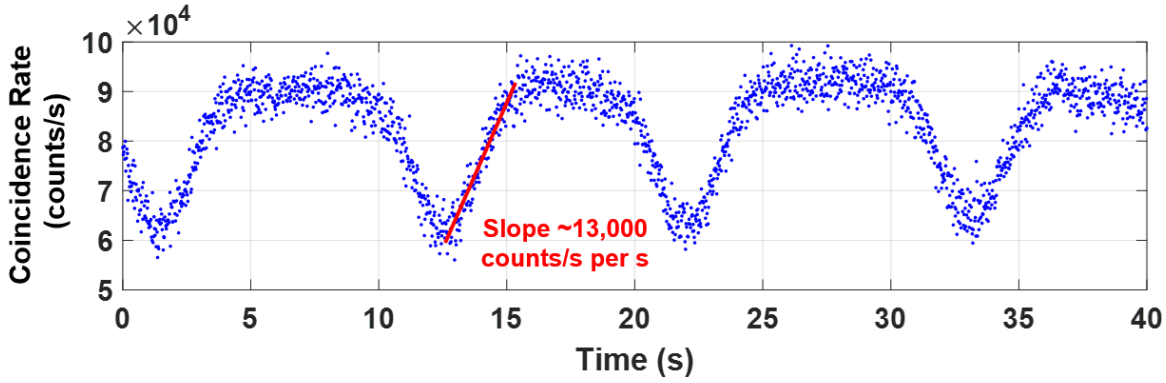

Figure 5 HOM timing discriminant characterization. Measured coincidence counts vs. delay as one source was scanned relative to the other. Delay line was scanned 10 ps back and forth over the HOM dip at a rate of 1 ps/s. The sources were locked using a local phase-locked loop operating from a strong signal derived from a mixer. The delay was scanned back and forth through the dip, creating the multiple dips in the 40-s time series. For a control point operating on the side of the HOM dip, this implies a discriminant sensitivity of ~13,000 counts/s for a 1-ps change in relative time delay.

Tests were conducted with an average signal flux of ~10^7 counts/s. For a random coincidence rate of ~10^5 counts/s given the ~1-% slot occupation probability, there will be ~1000 coincidence counts on average in a 10-ms control window. At an operating point on the side of the dip with ~750 coincidence counts in the 10-ms control interval, there would be ~$\sqrt{750}$~27 count fluctuation. For the measured discriminant slope of 130 counts per 10 ms interval per ps of timing delay (130 counts/10 ms/1 ps), this implies a timing control uncertainty of ~27/130=0.2 ps. A jitter of this magnitude, on the order of 20 % of the ~1-ps photon duration, should be sufficient for successful entanglement swaps.

This type of analysis can be used to determine the necessary strength of the strong supplemental timing control signal, and indicates that a minimum of 10^5 coincidence counts per second would be needed for the situation considered here. The signal to noise ratio could be enhanced significantly beyond this level without exceeding maximum detector count rates and/or overwhelming the weak quantum signal by utilizing a framed synchronization signal as discussed above to deliver timing pulses at predetermined slots. Note that the HOM discriminant technique shown here achieves near-quantum-limited synchronization, and is interesting to compare with other techniques [6].

After the initial timing discriminant characterization, the entangled photon sources were configured as shown in Figure 4 to operate from independent clock sources. The MLL pulse repetition rate is adjusted by using the frequency modulation input to the synthesizer to which the MLL is locked. A feedback control loop is implemented that derives an error signal from the HOM coincidence measurement and applies it to the frequency modulation input of the synthesizer. When locked, the frequency adjustment aligns one source to the other in both frequency (repetition rate) and phase (fine timing). Subsequent testing has focused on the control loop tracking capability. Additional work is planned to implement efficient acquisition techniques, but currently acquisition is facilitated by a 'person-in-the-loop' to enable tracking control when timing is close enough for tracking to function. Figure 6 shows this process.

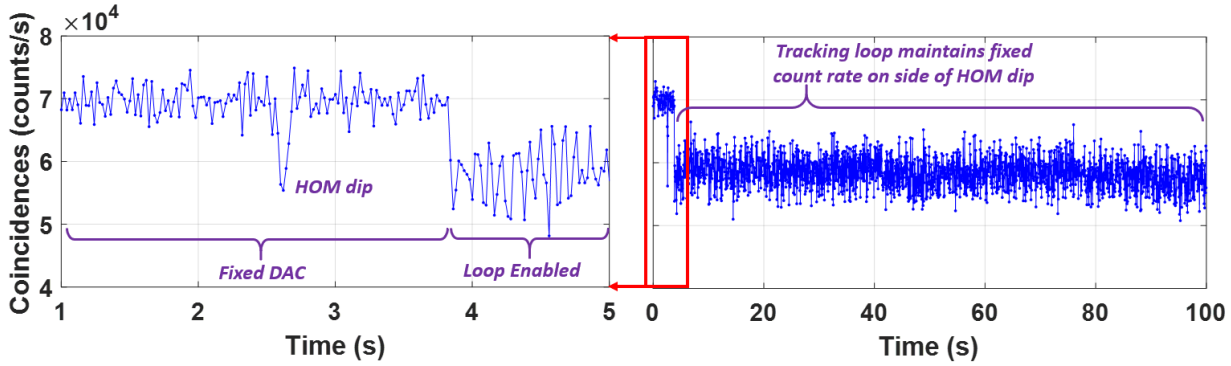

Figure 6 Transition from acquisition to tracking. The two sources were brought close in frequency so that the timing of one walked through the other slowly (e.g., relative delay changes by 1000 ps every 25 s for 1/40-Hz frequency offset at 1 GHz). The coincidence count rate showed the usual HOM dip, and the control loop feedback was enabled ~1 s after passing through the dip. The loop pulled the secondary source frequency (and hence delay), returning to the side of the HOM dip. The source remained aligned to the primary for the remainder of the 100-s test.

These initial results were collected using a simple feedback control loop that based the feedback voltage going to the frequency modulation input to a synthesizer on the measured coincidence signal. This type-1 phase locked loop nulls out a phase offset, but not a frequency offset (type-2 loop) or a frequency rate of change (type-3) [16, 17]. For control over the range of orbital motion considered here with a space-to-ground propagation delay, a type-3 control loop is necessary, and will yield, in principle, a residual phase (timing) error related to the Doppler curvature shown in Figure 2. It is estimated that such residuals should be negligible (<0.1 ps). The function of such a type-3 control loop is to monitor and anticipate the frequency and frequency rate-of-change based on the dynamic control loop output so that the secondary source will track the primary given the relatively infrequent (~10 ms) updates compatible with the space-to-ground propagation delay. Figure 7 shows data collected during a test of the type-3 control loop using profiles representative of the expected Doppler motion, but over much smaller ranges.

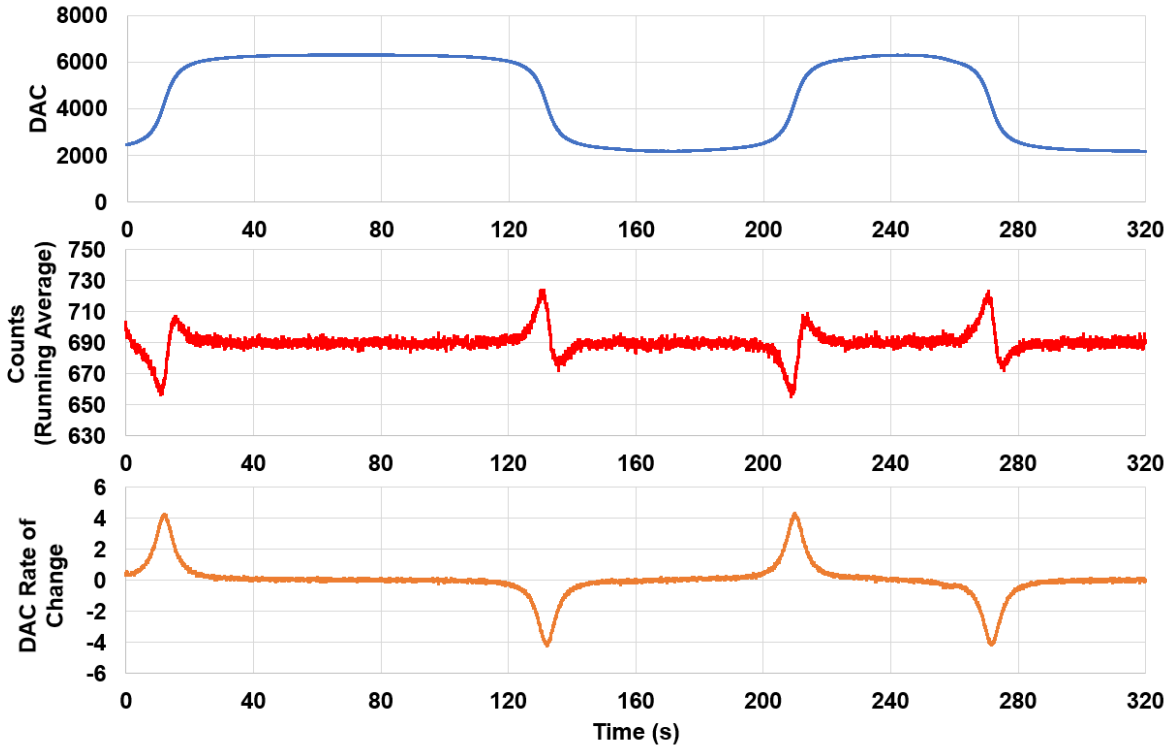

Figure 7 Control loop telemetry recorded by the FPGA during tracking while the frequency of the primary source was tuned over a ~16-ppb range at a peak rate of 1.5 ppb/s and curvature of 0.3 ppb/s^2. Blue points (top plot) show the 16-bit DAC value, which is updated by the FPGA every 10 ms. Relationship between DAC and frequency is ~4 mHz/DAC step. Red points (middle plot) show a ~1-s running average of the FPGA's recorded coincidence counts in each 10-ms interval. Orange points (bottom plot) are the FPGA's measure of the DAC rate of change (change in DAC per 10-ms update interval). The FPGA uses the DAC values to update a current average DAC setting (type-2 control loop operation) and the DAC rate of change to approximately null out the frequency rate of change (type-3 control). Results shown were collected in order to optimize this nulling process, and further optimization is planned. Note that a coincidence count offset of 30 counts corresponds to ~0.3 ps.

Work is underway to extend the Doppler range and rate capability of the control loop to be suitable for the orbital situations shown in Figure 2. Because the feedback control DAC does not have the range to directly cover the full ±23-ppm Doppler range, a technique for tuning over a wider range must be implemented. One potential method is for an outer control loop to monitor the DAC voltage and tune the synthesizer so that the DAC does not go beyond its 16-bit range. This tuning must be done carefully with small and steady steps because of the limited control bandwidth. Another relevant tool is the use of pre-compensation. Because orbits can be well predicted, the sources themselves can be predictively tuned to remove much of the relative Doppler, leaving the control loop to correct for the small residual errors due to uncertainty in orbits and other effects (such as unpredictable optical path length through the atmosphere). It is expected that the testbed will increase in fidelity to test for other effects such as intensity fluctuations due to atmospheric propagation, and changing round trip time delay during the duration of an orbital session.

While the focus of this work is on synchronization, the goal is to enable entanglement distribution, and it is important to confirm that synchronization is maintained for the entangled photons themselves. Figure 8 shows a HOM fourfold coincidence dip collected with the timing control loop operating while separate fiber delay lines (see Figure 4) slowly vary the delay of photons from one entanglement source relative to the other to reveal a HOM dip. For this HOM measurement, linear polarizers were placed on all entangled photons. One photon from each pair was sent to a 50/50 beam splitter for HOM interference, and the other photon was detected on an independent channel. This was an early test with the type-1 control. Note that because of the good synchronization control, data could be collected for longer averaging periods, with 10-s per point used here.

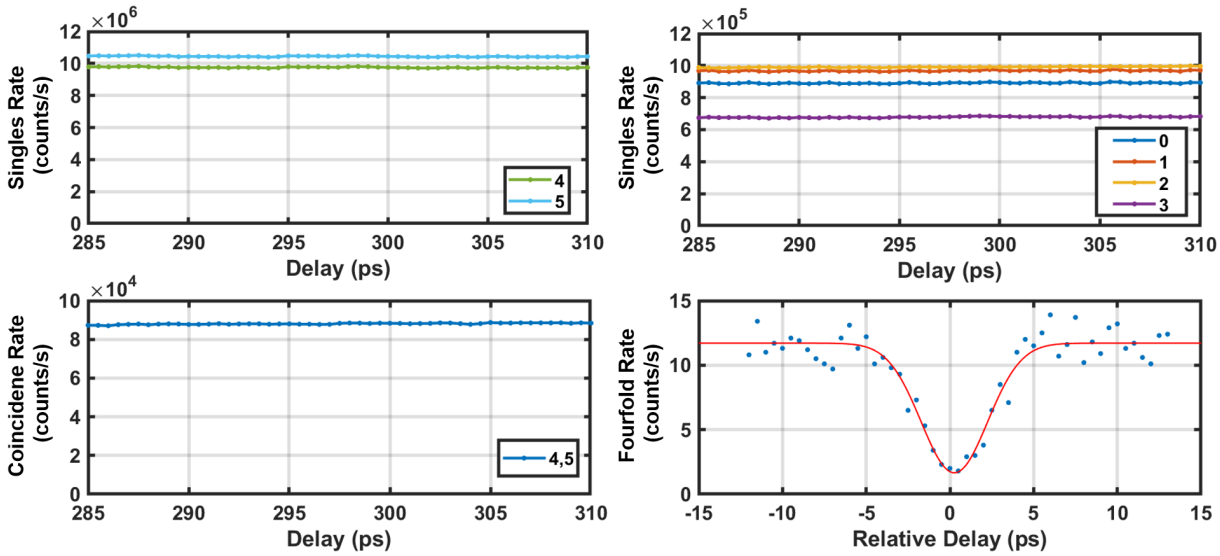

Figure 8 Quantum HOM measurement with independent synchronized sources. Upper left plot shows the 'singles' count rate (counts on detector channels 4 and 5, see labels in Figure 4) for the 775-nm synchronization signal. Lower left figure shows the detector channel 4-to-5 coincidence count rate. The operating point was on the side of the HOM dip, where the coincidence rate was reduced from its expected peak of $\sim 10^7(10^7/10^9)=10^5$ counts/s. The nearly-constant coincidence rate shows the control loop was maintaining synchronization during the measurement time while the delay line controlling the 1550-nm entangled photons was stepped in 0.5-ps steps, with a 10-s per step integration time. The upper right plot shows the singles count rate from each of the four detectors used in the HOM measurement, while the lower right plot shows the four-fold coincidence rate with the quantum HOM dip. The red curve is a fit to a profile with a visibility of 0.86.

5. SUMMARY

This work has examined a method for precision synchronization suitable for long-distance quantum networking, and demonstrated its feasibility in a laboratory testbed. The method uses mode-locked laser repetition rate control as the primary mechanism to correct for changes in range and rate due to orbital motion. It uses a sensitive HOM-based timing discriminant which minimizes the photon flux needed for synchronization. Results described in this paper show successful tracking over a 16-ppb Doppler range at a peak Doppler rate of change of 1.5 ppb/s and a curvature of 0.3 ppb/s^2, and work is underway to explore operation over larger Doppler ranges, and to include an automated acquisition capability. The technique can be extended and adapted to many different quantum networking and other precision synchronization applications.

ACKNOWLEDGEMENT

The authors thank Dr. Babak Saif of NASA Space Communications and Navigation (SCaN) for the suggestion to consider the dual-uplink architecture, and for discussions about methods for achieving precision synchronization for quantum networking applications.

DISTRIBUTION STATEMENT A. Approved for public release. Distribution is unlimited.
This material is based upon work supported by the National Aeronautics and Space Administration under Air Force Contract No. FA8702-15-D-0001. Any opinions, findings, conclusions or recommendations expressed in this material are those of the author(s) and do not necessarily reflect the views of the National Aeronautics and Space Administration.

REFERENCES

[1] C. Lee et al., "Bright, Waveguide-based Entanglement Sources for High-rate Quantum Networking," *Optica Quantum 2.0 Conference*, paper QTh4A.7 (2022).

[2] M. Aspelmeyer et al., "Long-Distance Quantum Communication With Entangled Photons Using Satellites," *IEEE J. Sel. Top. Quantum Electronics*, vol. 9, no. 6, pp. 1541-1551, Nov/Dec. 2003.

[3] N. Hardy, P. B. Dixon, and S. A. Hamilton, "Teleportation Fidelity Improvement with Quantum Memory," *Optica Quantum 2.0 Conference*, paper QM4B.4 (2022).

[4] R. Quan et al., "Demonstration of quantum synchronization based on second-order quantum coherence of entangled photons," *Scientific Reports*, 6:30453, 2016.

[5] M. Bodine et al., "Optical time-frequency transfer across a free-space, three-node network," *APL Photon.* 5, 076113 (2020).

[6] E. Caldwell et al., "The time-programmable frequency comb and its use in quantum-limited ranging," *Nature*, Vol. 610, pp. 667-673, 27 Oct. 2022.

[7] R. Lafler and R. Lanning, "Quantum Time Transfer For Freespace Quantum Networking," arXiv:2211.00737v1, 1 Nov. 2022.

[8] L. Sinclair et al., "Optical phase noise from atmospheric fluctuations and its impact on optical time-frequency transfer," *Phys. Rev. A*, 89, 023805 (2014).

[9] M. Taylor et al., "Effect of atmospheric turbulence on timing instability for partially reciprocal two-way optical time transfer links," *Phys. Rev. A*, 101, 033843 (2020).

[10] D. Boroson et al., "An Architecture for Synchronizing Photonic Bell State Measurements Across Lossy, Time-Varying Channels," *OSA Quantum 2.0 Conference*, paper QTh7B.18 (2020).

[11] N. Spellmeyer et al., "Free-space Forwarded-pump Entanglement Source Synchronization," *Optica Quantum 2.0 Conference*, paper QTh3A.4 (2022).

[12] H. Chen et al., "Hong–Ou–Mandel interference with two independent weak coherent states," *Chin. Phys. B*, 25, 020305 (2016).

[13] Y-S. Kim et al., "Two-photon interference with continuous-wave multi-mode coherent light," *Optics Express* Vol. 22, No. 3, pp. 3611-3620, 6 Feb. 2014.

[14] E. Moschandreou et al., "Experimental Study of Hong–Ou–Mandel Interference Using Independent Phase Randomized Weak Coherent States," *IEEE J. of Lightwave Tech.*, Vol. 36, No. 17, 1 Sep. 2018.

[15] A. Aragoneses et al., "Bounding the outcome of a two-photon interference measurement using weak coherent states," *Optics Letters*, Vol. 43, No. 16, pp. 3806-3809, 15 Aug 2018.

[16] F.M. Gardner, *Phaselock Techniques*, John Wiley & Sons, Third Edition, 2005.

[17] S. Golestan et al., "Advantages and challenges of a type-3 PLL," *IEEE Trans. Power Electronics*, vol. 28, no. 11, Nov. 2013, pp. 4985 – 4997.